Research Update: Behind the high efficiency of hybrid perovskite solar cells

Azhar Fakharuddin, Francesca De Rossi, Trystan M. Watson, Lukas Schmidt-Mende, and Rajan Jose

---

Research Update: Behind the high efficiency of hybrid perovskite solar cells

Azhar Fakharuddin,[1,2,a] Francesca De Rossi,[3,a] Trystan M. Watson,[3]
Lukas Schmidt-Mende,[1] and Rajan Jose[4,a]

[1]*Department of Physics, University of Konstanz, D-78457 Konstanz, Germany*
[2]*School of Chemical and Materials Engineering, National University of Sciences
and Technology, H-12, Islamabad, Pakistan*
[3]*College of Engineering, SPECIFIC – Swansea University, Bay Campus,
SA1 8EN Swansea, United Kingdom*
[4]*Nanostructured Renewable Energy Materials Laboratory, Universiti Malaysia Pahang,
26300 Kuantan, Malaysia*

Perovskite solar cells (PSCs) marked tremendous progress in a short period of time and offer bright hopes for cheap solar electricity. Despite high power conversion efficiency >20%, its poor operational stability as well as involvement of toxic, volatile, and less-abundant materials hinders its practical deployment. The fact that degradation and toxicity are typically observed in the most successful perovskite involving organic cation and toxic lead, i.e., $CH_3NH_3PbX_3$, requires a deep understanding of their role in photovoltaic performance in order to envisage if a non-toxic, stable yet highly efficient device is feasible. Towards this, we first provide an overview of the basic chemistry and physics of halide perovskites and its correlation with its extraordinary properties such as crystal structure, bandgap, ferroelectricity, and electronic transport. We then discuss device related aspects such as the various device designs in PSCs and role of interfaces in origin of PV parameters particularly open circuit voltage, various film processing methods and their effect on morphology and characteristics of perovskite films, and the origin and elimination of hysteresis and operational stability in these devices. We then identify future perspectives for stable and efficient PSCs for practical deployment. © 2016 Author(s). All article content, except where otherwise noted, is licensed under a Creative Commons Attribution (CC BY) license (http://creativecommons.org/licenses/by/4.0/). [http://dx.doi.org/10.1063/1.4962143]

I. INTRODUCTION

Solar cells made using organometallic halide perovskites ($CH_3NH_3PbX_3$, where X = I, Cl and Br)—a next generation solution processable low cost material—have reached a certified power conversion efficiency (PCE) ~22.1%,[1] in merely 4 yr since their first viable solid-state device in 2012.[2] In a typical perovskite solar cell (PSCs) architecture, a thin perovskite layer is stacked between an electron selective contact (ESC) and a hole selective contact (HSC) making a heterojunction cell.[3–7] The choice of selective contacts and the subsequent arrangement of the perovskite layer determines device designs of PSCs ranging from mesoporous to a thin film like, conducting scaffolds based PSCs to electrically insulating ones, and also from bi-interfacial to single interfacial PSCs. All these devices showed a photoconversion efficiency ≥15% in a total active material thickness of <1 μm, thanks to the high absorption coefficient (10^3–10^4 cm^{-1}) of $CH_3NH_3PbX_3$ coupled with its high charge carrier mobility (2–66 cm^2 V^{-1} s^{-1}).[3,8]

---

[a]Authors to whom correspondence should be addressed. Electronic addresses: azhar-fakhar.uddin@uni-konstanz.de; f.derossi@swansea.ac.uk; and rjose@ump.edu.my

4, 091505-1

From a material perspective, the case of PSCs is very fascinating: the $CH_3NH_3PbX_3$ has a tunable bandgap ~1.55 to 2.5 eV[9,10] and can be processed from solutions at low temperatures <150 °C.[11–14] The $CH_3NH_3PbI_3$ perovskite undergoes rapid crystallization;[15,16] therefore, a strict control is often required for a desirable film morphology and properties thereby. High quality films possess properties similar to that of inorganic semiconductors such as diffusion length of 0.1–1.9 μm, low trap state density ~10^{10} cm^{-3}, and a carrier lifetime of ~270 ns which coupled with their low binding energy ≤5 meV makes them an ideal candidate for solar cells.[17–19] However, the presence of lead (Pb) makes them toxic which accounts for ~0.55% of total material,[20] an amount slightly higher than the allowed limit set by European Restriction on Hazardous Substances. Furthermore, this material demonstrated ionic-electronic behavior leading to hysteresis in the devices,[21–23] unless prepared with extreme care. In addition, these devices yet have to show a stable performance comparable to that of silicon and thin film solar cells, primarily because the initial precursors used to synthesize $CH_3NH_3PbX_3$ are water soluble; and therefore, moisture sensitive. It is noteworthy that the hysteresis and stability of PSCs as well as their PV performance largely depend on the preparation method, synthesis conditions as well as the selective contacts; therefore, efficient device fabrication requires appropriate knowledge of these various factors.

The main aim of this article is to provide insights into the contribution of various material constituents towards the PV performance in PSCs. Therefore, properties of $CH_3NH_3PbX_3$ are correlated to its crystal structure in Sec. II. As the film processing and the device architecture largely influence photovoltaic operation, we provide insights into the working mechanism of the various PSC architectures, in particular, the role of a scaffold holding the perovskite crystals and the origin of open circuit voltage in PSCs. Various film-processing methods are detailed followed by a discussion on the key issues that need to be solved for a commercially deployable device such as stability and hysteresis.

II. STRUCTURAL PROPERTIES OF HYBRID PEROVSKITES

Perovskite crystals are typically expressed by a general formula ABX_3, where A and B are 12-fold and 6-fold coordinated cations, respectively, and X is generally a halogen or oxygen.[24,25] The 6-fold coordination of the B ion makes BX_6 octahedra which are ideally corner shared along all the three crystallographic axes (TiO_6 and PbI_6 octahedra in Figure 1) and the dodecahedral interstice thereby produced is filled by the A cation. To have the above structure, the ions forming it should have a certain size distribution such that $\frac{R_A + R_X}{\sqrt{2}(R_B + R_X)} = t$, where the $R's$ are the Goldsmith ionic radius of the respective ions and the term t is referred as the tolerance factor, which is usually in the 0.75–1 range, i.e., to tolerate a perovskite phase, the condition $R_A > R_B > R_X$ is always required.[3]

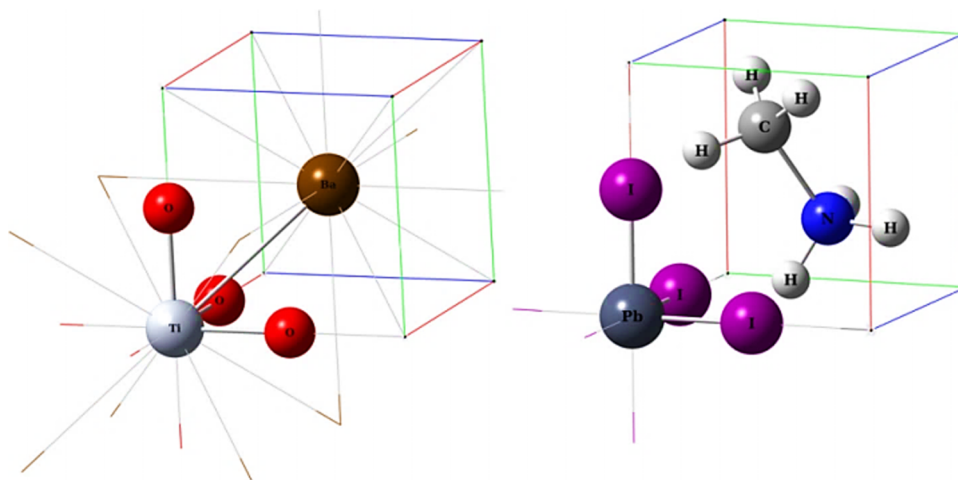FIG. 1. Symmetric atomic positions of $BaTiO_3$ (left) and $MAPbI_3$ (right) in a perovskite lattice. The bond lengths are not optimized. The arrows indicate the lattice translation vectors.

The closer the tolerance factor is to unity, the more stable corner shared cubic perovskite forms for which $R_A \sim 1.4\ R_B + 0.4\ R_X$. Lower values of t lead to transition to lower crystal symmetries than cubic as well as the corner sharing octahedra changes to edge sharing and ultimately to face sharing octahedra.[26] In the case of non-ideal tolerance factor ($t = 1$), i.e., when the sizes of A, B, and X ions do not match well for a perfect octahedra, the BX_6 octahedra undergoes a tilting and the A ion also consequently displaced—which gives electrical polarity to perovskite crystals and is the source of ferroelectricity in perovskite crystals. This octahedral tilting and subsequent phase transition are the source of diverse range of electronic properties of perovskites.[27]

The inorganic oxide perovskites forms a large number of chemical entities such as $A^{2+}B4 + O_3^{2-}$ and $A^{2+}(B_{0.5}^{5+}B_{0.5}'^{3+})O_3^{2-}$ as one would find out elements to form a combination giving an acceptable tolerance factor and charge balance. However, the halide analogues do not offer that enormity because (i) size of the halogen ions, excluding fluorine, is much higher than that of oxygen—they demand larger ions to be at the centre of the octahedral and even larger ones at the dodecahedral positions, and (ii) halogen bears a single negative charge against two of the oxygen; therefore, A and B ions with a total valence of +3 only can give rise to an electrically neutral perovskite. These size and charge requirements limits the halide perovskites to be realized from methylammonium ion (MA, $R_A \sim 1.81$ Å, charge +1), C_S ($R_A \sim 2.7$ Å, charge +1), and formamidinium ion (FA, $R_A \sim 2.79$ Å, charge +1) for the A site;[28] heavier group 14 elements such as Pb^{2+}, Ge^{2+}, Sn^{2+}, alkaline earths, and bivalent rare-earth to be at its B site. A detailed account on the chemistry of formation of hybrid perovskite is published elsewhere.[25] One would observe from their tolerance factors that the organic/inorganic halides form perovskite structure with distorted octahedra (Table I); nature of their deviation and classification based on the octahedral tilting is summarized in a recent account.[29] Consequently, existence of ferroelectric molecular domains in the methylammonium lead halide perovskite ($MAPbX_3$) is predicted by *ab initio* molecular dynamic simulations.[30]

The difference in properties of the oxide perovskites, such as $BaTiO_3$ (Figure 1(a)), and halide perovskite, such as $MAPbX_3$ (Figure 1(b)), could be well understood from the difference in their chemical structure as demonstrated in Figure 1.

The A site in the inorganic perovskite is occupied by a single atomic ion whereas it is occupied by a functional group (MA ion) in the hybrid phase. In addition, one would see that, by the virtue of its symmetry, the MA ion is polar and would additionally contribute to the dielectric constant offered by tilted of PI_6 octahedra. The inorganic phase has a centre of symmetry; therefore, they do not possess certain optical properties such as photoluminescence. On the other hand, the hybrid phase is not a centrosymmetric crystal, thereby showing photoluminescence and extending

TABLE I. Tolerance factor and band gap of halide perovskites and PV parameters employing them as light harvesters. Most of the PSCs employ Spiro and TiO_2 as HSC and ESC, respectively, unless stated otherwise.

Absorber	Tolerance factor	Band gap	PV parameters[a]
$CH_3NH_3PbI_3$	0.83	1.55	**17.9%** (21.0, 1.11 V, 0.76 FF)[46b]
$CH_3NH_3PbI_{3-x}Cl_x$	0.83–0.85	1.85	**19.3%** (22.7, 1.13 V, 0.75 FF)[47]
$CH_3NH_3PbCl_3$	0.85		
$CH_3NH_3PbI_{3-x}Br_x$	0.81–0.83	1.6–2.3	**16.5%** (19.6, 1.1 V, 0.76 FF)[48]
$CH_3NH_3PbBr_{3-x}Cl_x$	0.81–0.85	~2.2	**2.7%** (4, 1.5 V, 0.46 FF)[49]
$CH_3NH_3PbBr_3$	0.81	2.3	**7.5%** (6.04, 1,61 V, 0.77 FF)[50c]
			11.4% (14.1, 1.11 V, 0.73 FF)[51d]
$CsPbI_3$	0.81[28]	1.65	**2.9%** (12, 0.8 V, 0.30 FF)[52]
$FAPbI_3$			
$(FAPbI_3)_{1-x}(MAPbBr3)_x$			**20.8%** (24,6, 1.16 V, 0.73 FF)[53]
$Csx(MA_{0.17}FA_{0.83})_{(100-x)}Pb(I_{0.83}Br_{0.17})_3$			**21.1%** (23.5, 1.15 V, 0.78 FF)[54]
$CH_3NH_3SnI_3$	0.97	1.30	**6.4%** (16.8, 0.88 V, 0.42 FF)[55]

[a]The IV parameters follow the order (PCE (J_{SC}, V_{OC}, and FF)). The unit for J_{SC} is mA/cm^2 and not included to shorten the text.

[b]A corresponding device employing $MAPbBr_3$ resulted in PCE 4.4% (4.4, 1.3 V, 0.75 FF).

[c]Employs PEDOT:PSS and ICBA as HTM/ETL.

[d]PTAA and TiO_2.

optoelectronic functionalities to the perovskite crystals. Besides symmetry elements, motion of the A site ion also contributes to their optical non-linearities.[31–33] Allowable motion of the ions in the inorganic phase is translatory, whereas the A site ion in the hybrid phase would additionally rotate in the presence of an electric field, magnetic field, or light. This peculiar geometry of the $MAPbX_3$, that is a tilted PI_6 octahedra with a polar entity at the A site, would offer changes in the total polarity of the crystal as the A-site ion is rotated—which is the source of the giant optical non-linearities of the $MAPbX_3$ crystals. Consequently, there are considerable inconsistencies in the measured dielectric constant of the methylammonium lead halide perovskite. For instance, its static dielectric constant is determined to be 6.5,[34,35] 70,[36] and over 1000.[37] A low temperature measurement under dark employing small perturbation condition is expected to provide accurate values.

The energy for molecular rotation is on the order of few meV, which thermal quanta at the normal temperatures would provide; thereby offering significant challenges in precisely determining the crystal structure parameters of hybrid perovskites. Considerable efforts have been devoted in determining the crystal structure parameters of the $MAPbX_3$ from X-ray diffraction measurements and subsequent Rietveld refinement; however, the refined structure deviates considerably from the perovskite geometry, mainly the MA ion lacks a 12-fold symmetry in many of the refined structures.[8,38–40] Besides the inferior X-ray scatterability of light elements such as H, N, and C, accurate determination of the Debye-Waller instability also contributed to such inconsistency. One of the potential remedies could be depending on diffraction by high energy radiations.[41]

A. Electronic properties of halide perovskites

As a solar cell material, emitting states of the $MAPbX_3$ are extremely important. Considerable attention is devoted to understand the electronic band structure of hybrid perovskites from experimental measurements and quantum chemical calculations.[42–44] $MAPbX_3$ is a direct band gap semiconductor with two transitions at 760 and 480 nm. A general understanding is that top of the valence band in both of these transitions are composed of p-orbitals of I mixed with 6p and 6s orbitals of Pb; the bottom of the conduction band is formed by σ-antibonding orbitals of 6p of Pb and 5s of I and π-antibonding orbitals of 6p of Pb and 5p of I.[24,45] No contribution from the MA ion has been detected on the band edges and band gap, and their energy levels fall within the bands.

Now the significant question from a structural point of view of the halide perovskite is the origin of photovoltaic action in PSCs. Low exciton binding energies (≤ 5 meV) of halide perovskites determined experimentally from optical measurements[36] and theoretically by DFT[30] point out that charge generation is non-excitonic. Further, many experiments reveal the ionic character of this perovskite.[56,57] The mobile nature of the MA ion, its positive charge, and the fact that they are not involved in the charge injection/dynamic states in the electronic bands of this crystal would hint that they provide an ion conducting pathway. The very low fill factor observed in the $CsPbI_3$ PSC (Table I) could be another supporting evidence for the role of the mobility of the A-site ions contribution to the successful photovoltaic action. On the other hand, large electron density of lead and iodine, existence of ferroelectric molecular domains, and the fact that light absorption only involves the PbI_6 octahedra would lead to think that they are the electron conducting pathway. Large difference in PCE of the PSCs fabricated between $MAPbI_3$ and $CsPbI_3$ (Table I) would additionally hint the role of the polar-and-mobile functional group entity at the A site rather than the relatively fixed molecular ion (Cs) and their subsequent higher order optical susceptibility (non-linearity) on the PV action.

III. DEVICE DESIGNS AND PHOTOVOLTAIC ACTION IN PEROVSKITE SOLAR CELLS

Historically, PSCs evolved from dye-sensitized solar cells (DSCs) where a dye is replaced with a perovskite absorber ($CH_3NH_3PbI_3$ or $CH_3NH_3PbBr_3$) of 15–20 times higher absorption coefficient (10^3–10^4 cm^{-1}) on a mesoporous TiO_2 film (~10 μm) and resulted in PCE ~3.9%.[58] Although the PCE was subsequently increased to 6.5% in a thinner TiO_2 film (~4 μm), the PSCs showed a lifetime of few hours only, as the perovskite layer dissolved in the liquid electrolyte employed as a hole transport media.[59]

A viable device is only shown when the liquid electrolyte is replaced by a solid-state HSC, e.g., 2,2′,7,7′-tetrakis-(N,N-*p*-dimethoxy-phenylamino)-9,9′-spirobifluorene (spiro-OMETAD) resulting in PCE ~9.7%.[2] The higher absorption coefficient of $CH_3NH_3PbX_3$ coupled with its high charge carrier mobility (2–66 cm^2 V^{-1} s^{-1})[8] allowed TiO_2 layer to be 300–500 nm, which together with controlled perovskite crystallization further improved the performance up to ~15%.[15,60] The state-of-the-art performance in PSCs (19%-21%)[46,53,54,61,62] is obtained by (i) chemically tailoring $CH_3NH_3PbX_3$ by incorporating FA and/or Cs along with MA and also by introducing mixed halide salts such as PbBr and PbI,[54] (ii) optimized ESC and HSC for efficient charge extraction,[47] and (iii) an optimized morphology of perovskite layer. Although high performance >20% is typically reported in devices employing a mesoporous scaffold (thickness ~150 to 300 nm), an excellent performance 18%–19% is also reported in thin-film versions of PSCs[47,63–65] employing a compact layer as a selective contact.

In a typical device architecture, a ~300 nm thick perovskite film between ESC and HSC creates two interfaces, viz., ESC-perovskite and HSC-perovskite.[72] The PSCs offer a wide variety of device designs, more than any other class of solar cell technology, which is determined by the charge (n- or p-type), morphology (mesoporous or a flat thin film), and electrical properties (conducting or insulating) of the ESC/HSC on conducting substrate making it a n-i-p or p-i-n, p-n or n-p, meso-porous or planar, and mesoporous or meso-superstructured PSC (MSSCs), respectively, as shown in Fig. 2. A report by Lee *et al.*[73] showed that the PSCs—contrary to the initial understanding of the need of a selective contact for charge separation and transport—can also work efficiently with an insulating scaffold (Al_2O_3). This evidenced ambipolar charge transport in perovskite film with balanced electron and hole diffusion lengths up to ~1 μm.[18,74] In fact, the devices employing insulating scaffolds demonstrated higher carrier lifetime compared to a TiO_2 scaffold counterparts
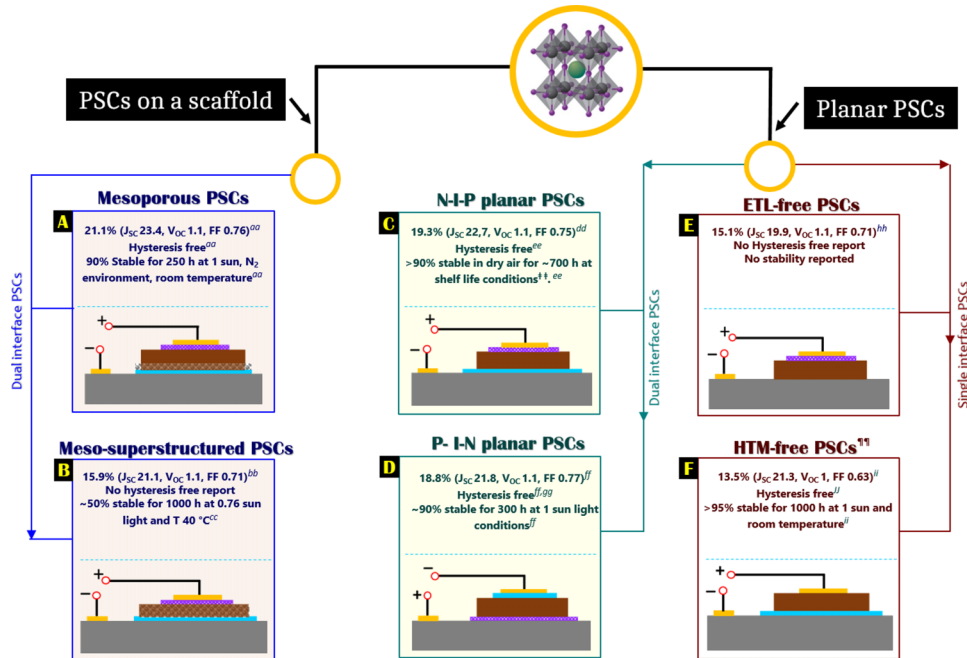

FIG. 2. The common device architectures of perovskite solar cells are classified in two major categories: mesoporous, employing a scaffold, and planar, employing a thin flat layer. The mesoporous scaffold can be electrically conducting such as TiO_2 and ZnO or insulating such as Al_2O_3 and ZrO_2. The planar PSCs can be divided in two sub-categories: (i) dual interface PSCs, employing a perovskite layer between ESC and HSC, and (ii) single interface PSCs employing only one of the two selective contacts. The inset of each figure also shows highest performance reported for each architecture and whether or not hysteresis-free and a stable performance is achieved. The crystal structure of perovskite is adapted with permission from M. Grätzel, Nat. Mater. **13**, 838–842 (2014). Copyright 2014 Nature Publishing Group.[145] ††, room temperature, room light; ¶¶, the device also employing monolithic PSCs (few micron thick carbon back contact is deposited over perovskite); *aa*, Saliba *et al.*;[54] *bb*, Wojciechowski *et al.*;[66] *cc*, Leijtens *et al.*;[67] *dd*, Zhou *et al.*;[47] *ee*, Correa Baena *et al.*;[68] *ff*, Zhu *et al.*;[64] *gg*, Bi *et al.*;[65] *hh*, Hu *et al.*;[69] *ii*, Wei *et al.*;[70] *JJ*, Wei *et al.*[71]
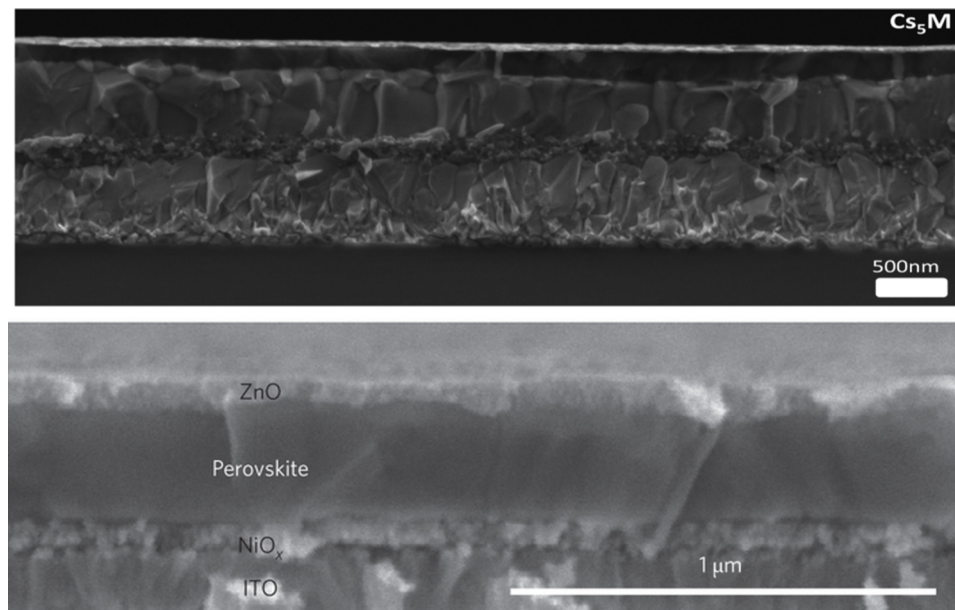
FIG. 3. A comparison of the various material constituents of state-of-the-art mesoporous[54] (top) and planar[79] (bottom) perovskite solar cells. Figures are reproduced with permission from Saliba *et al.*, Energy Environ. Sci. **9**, 1989-1997 (2016). Copyright 2016 The Royal Society of Chemistry and You *et al.*, Nat. Nanotechnol. **11**(1), 75-81 (2016). Copyright 2016 Nature Publishing Group, respectively.

due to TiO_2, which take part in charge collection, having far lower electron mobility, by many orders, than $CH_3NH_3PbX_3$ and also sub-band gap states that leads to interfacial recombination.[73]

Although initially the mesoporous PSCs (Fig. 2(a)) employed a scaffold of thickness 300–500 nm, it is quite recently that the thickness has dropped to less than its half, i.e., 100–200 nm,[46,54] primarily owing to improvement in perovskite film characteristics and also the understanding of the working mechanism of PSCs which is more thin-film like rather excitonic. It is therefore intriguing whether a mesoporous scaffold is required for an efficient device operation. The PSCs will however require a pin-hole free selective contact over conducting substrate to avoid charge recombination but it should also be thin enough not to add to charge transport resistance. Contrary to the initial reports on PSCs, the morphology of typical representative ESC films of high performing mesoporous and planar PSCs (Fig. 3) is now comparable, both made of nanoparticle of different sizes and employ a ~300 nm perovskite overlayer. This suggests a minor contribution of scaffold towards perovskite morphology, at least for a thinner mesoporous layer. However, it can still play a significant role in thicker scaffolds (≥300 nm), especially for insulating oxides where electron collection to selective contact takes place via perovskite. Nevertheless, when it comes to a stable device, the PSCs employing a mesoporous scaffold have shown higher stability compared to their planar rivals. Furthermore, although efficient charge collection is observed for single interface PSCs employing only one of the selective contacts (Figs. 2(e) and 2(f)), these devices are yet to show a hysteresis free and stable performance.[69,75–78]

A. Open circuit voltage in perovskite solar cells

The mechanism of photovoltaic action and the origin of V_{OC} in PSCs remain ambiguous so far. The contribution of selective contacts to V_{OC} in a wide variety of device designs is not fully understood, thereby making its working principle hard to generalize. Nonetheless, it is now convincing that the PSCs are not excitonic and the charge separation—owing to its low binding energy (<5 meV)—takes place inside the perovskite layer, even at room temperature. Regarding the V_{OC}, in general, its theoretical upper limit is limited by the bandgap (E_G) of the absorber (perovskite in this case) whereas the practically obtainable V_{OC} depends on (i) the energy level alignment that determines electron injection losses, and (ii) charge mobility which determines losses during charge

transport. For ideal interfaces in PSC (no loss in electron injection and no interfacial recombination) $E_G - qV_{OC}$ should be zero and qV_{OC}/E_G should be 100%.[49] Table II shows such ratio for the PSCs made using various perovskites: MAPbBr$_3$ (E$_G \sim$ 2.3 eV) typically demonstrate higher V$_{OC}$ (1.3–1.6 V) which is higher than that obtained in MAPbI$_3$ based PSCs ($\sim$1.1 V). Herein, the V$_{OC}$ upper limit is defined by the splitting of electron and hole quasi-Fermi levels of the perovskite, which is strongly influenced by the interfacing contact. For example, an increase of $\sim$0.22 V is observed when PCBM is replaced with ICBA (see Table II), an ESC with $\sim$200 meV higher CB edge. Similarly, for a given perovskite and HSC, a drop of $\sim$0.3 V in V$_{OC}$ is observed when Al$_2$O$_3$ is replaced by a TiO$_2$ layer. This is due to the different device architecture and working mechanism of the two devices. In Al$_2$O$_3$ based PSCs, the electrons are carried to the selective contact by the perovskite layer itself, and the splitting of Fermi levels is determined by MAPbI$_3$ only, which owing to its high charge mobility and high dielectric constant results in a higher V$_{OC}$. In the case of TiO$_2$, electron injection takes place at TiO$_2$–MAPbI$_3$ interface to an energy level determined by the traps states in TiO$_2$ bandgap. Due to the offset between the CB of TiO$_2$ and MAPbI$_3$, the splitting of quasi-Fermi level of perovskite is now relatively smaller resulting in a lower V$_{OC}$. This can also explain typically higher V$_{OC}$ in planar PSCs compared to a mesoporous counterpart (both made using TiO$_2$) as the voltage loss (due to energy level offset) at the TiO$_2$–MAPbI$_3$ interface is expected to be smaller for a thin TiO$_2$ layer than a rival mesoporous.[73] As the effect of thin flat layer on splitting of quasi-Fermi levels of perovskite seems less significant, it could explain a similar V$_{OC} \sim$ 1.1 V for SnO$_2$ and TiO$_2$ despite a $\sim$300 meV lower CB edge of the former, for a given perovskite.[63] Higher electron mobility of SnO$_2$ and its lesser surface defects[80–82] compared to TiO$_2$ are two other factors that helped obtaining a similar V$_{OC}$ to TiO$_2$.

The V$_{OC}$ is also influenced by the HOMO level of the HSC and also its hole mobility. Table II shows systematic increase in V$_{OC}$ for HSC with deeper HOMO levels; it increased from 1.05 V to 1.51 V when P3HT is replaced with PIF8-TAA (see a comparison of their HOMO in Table II).[83] The increment in the V$_{OC}$ for the latter is nearly equal to the energy level difference of the two HSCs employed. A similar trend is noted by Ryu *et al.*;[84] the V$_{OC}$ increased $\sim$0.11 V upon employing HSC with deeper HUMO level. However, the HUMO level is not the only factor that influences the V$_{OC}$. In a comparison by Edri *et al.*,[49] (Table II) PCBM despite its deeper HUMO level (-6.1 eV) than PDI (-5.8 eV) demonstrated $\sim$0.24 $>$ V lower V$_{OC}$. This can be understood from the fact that the hole mobility of PCBM (10^{-2}–10^{-3} cm^2 V^{-1} s^{-1}) is two orders of magnitude lower than PDI ($\sim$2.1 cm^2 V^{-1} s^{-1}). Therefore, in order to obtain a higher V$_{OC}$ in PSCs, not only the energy level alignment of selective contacts to perovskite is necessary but also their superior charge mobility to avoid losses occurring during charge transport.

IV. PROCESSING OF PEROVSKITE FILMS

In a typical procedure, fabrication of PSCs involves the deposition of perovskite thin films as well as ESC and HSC via solution processing that, in addition to the high efficiency reported for these devices, offers routes for cost effective device fabrication. The processing of perovskite films, typically CH$_3$NH$_3$PbI$_3$, involves stoichiometric reaction of an organic halide, typically methylamine, with a metal halide such as PbI$_2$ (CH$_3$NH$_3$I + PbI$_2 \rightarrow$ CH$_3$NH$_3$PbI$_3$). The crystallization of CH$_3$NH$_3$PbI$_3$ starts at room temperature and is associated with a color change; upon reacting with CH$_3$NH$_3$I, the yellow colored PbI$_2$ films immediately changes to light brown (indicating start of crystallization) which turns dark brown upon annealing, thereby demonstrating a complete transformation to perovskite. Perovskite crystallization is a crucial step and a sharp control on it is required to achieve smooth, highly crystalline films which are thick enough to absorb maximum incident light and yet thin enough to enable complete charge collection, pinhole-free as to avoid a direct contact between HSC and ESC, with less grain boundaries in its crystals.

Various synthesis routes are employed to tune the film characteristics, such as single step (SS) and double step (DS) depositions, dual source evaporation (DSE), and vacuum assisted vapor deposition (VAVD). Both the solution-based SS and DS routes allow for perovskite films with remarkable morphology and crystallinity and cells with efficiency beyond 20%. Currently, the SS—mostly in its solvent engineering variants described below—seems the preferred method for

TABLE II. A comparison of state-of-the-art open circuit voltage obtained using various halide perovskites in conjunction with a diverse range of electron and hole selective contacts. The CB and VB edges for MAPbI$_3$ and MAPbBr$_3$ are ($-3.9/-5.4$) eV and ($-3.4/-5.6$) eV, respectively. ■, CB/conduction band edge of ESC; ▲, HUMO of HSC.

V$_{OC}$ (V)	J$_{SC}$ (mA/cm^2)	FF	PCE (%)	ESC	Device architecture	HSC	Band edges (CB/HUMO)	Hole mobility (cm^2 V^{-1} s^{-1})	Device	qV$_{OC}$/E$_G$ (%)	E$_G-q$V$_{OC}$ (eV)	Reference
1.11	21.00	0.76	17.9	c,m-TiO$_2$	Cs$_x$(MA$_{0.17}$FA$_{0.83}$)$_{(100x)}$Pb($I_{0.83}$Br$_{0.17}$)$_3$	Spiro-OMETAD	-4.4■/-5.11▲	10^{-3}–10^{-4},[85]	Mesoporous PSC	72	0.44	Saliba et al.[54]
1.13	22.7	0.75	19.3	Y-TiO$_2$[a]	CH$_3$NH$_3$ PbI$_{3-x}$Cl$_x$	Spiro-OMETAD	-5.11▲	10^{-3}–10^{-4},[85]	n-i-p planar	61	0.72	Zhou et al.[47]
1.00	1.14	0.40	0.5	TiO$_2$	MAPbBr$_3$	PDI[b]	-5.8▲	2.1	MSSC	48	1.20	
1.30	1.08	0.40	0.6	Al$_2$O$_3$	MAPbBr$_3$	PDI[b]	-5.8▲	2.1		56	1.00	Edri et al.[86]
1.29	6.60	0.70	5.9	TiO$_2$	MAPbBr$_3$	P-TAA[c]	-5.14▲	>0.1,[86]	Mesoporous PSC	56	1.01	Ryu et al.[84]
1.36	6.30	0.70	6.0	TiO$_2$	MAPbBr$_3$	PF8-TAA[d]	-5.44▲	4×10^{-3}		59	0.94	
1.40	6.10	0.79	6.7	TiO$_2$	MAPbBr$_3$	PIF8-TAA[e]	-5.51▲	4×10^{-2}		61	0.90	
1.04	21.3	0.73	16.2	TiO$_2$	MAPbI$_3$	P-TAA	-5.14▲	>0.1,[86]		67	0.51	
0.92	8.90	0.56	4.6	TiO$_2$	MAPbI$_3$	PF8-TAA	-5.44▲	4×10^{-3}		59	0.63	
1.04	19.0	0.46	9.1	TiO$_2$	MAPbI$_3$	PIF8-TAA	-5.51▲	4×10^{-2}		67	0.51	
1.50	4.00	0.47	2.7	Al$_2$O$_3$	MAPbBr$_{3-x}$Cl$_x$	CBP[f]	6–6.2▲[87]		MSSC	70	0.73	Edri et al.[49]
1.09	8.5	0.79	7.3	TiO$_2$	MAPbBr$_3$	P3HT	-5.0▲	>0.1,[86]	Mesoporous PSC	47	1.21	Heo et al.[83]
1.35	8.4	0.82	9.3	TiO$_2$	MAPbBr$_3$	P-TAA	-5.14▲	4×10^{-3}		59	0.95	
1.51	8.4	0.82	10.4	TiO$_2$	MAPbBr$_3$	PIF8-TAA	-5.51▲	4×10^{-2}		67	0.65	
1.38	5.2	0.78	5.6	PCBM[g]	MAPbBr$_3$	PEDOT:PSS	-3.9■/-5.3▲		p-i-n inverted	60	0.92	Wu et al.[50]
1.61	6.04	0.77	7.5	ICBA[h]	MAPbBr$_3$	PEDOT:PSS	-3.7■/-5.3▲			70	0.69	Wu et al.[50]

[a]Y-TiO$_2$: Yitrium doped TiO$_2$.
[b]PDI: N,N′-dialkyl perylenediimide.
[c]P3HT: poly-(3-hexyl)thiophen.
[d]P-TAA: oly[bis(4-phenyl) (2,4,6-trimethylphenyl)amine].
[e]PIF8-TAA: poly-indenofl uoren-8-triarylamine.
[f]CPB: 4,4′-bis(N-carbazolyl)-1,1′-biphenyl.
[g]PCBM: phenyl-C61-butyric acid methyl ester.
[h]ICBA: 1′,1,4′,4″-tetrahydro-di[1,4]methanonaphtaleno[1,2:2′,3′,56,60: 2″,3″][5,6] fullerene-C60.

perovskite deposition at lab scale. Likely, it is also the more promising candidate to be employed in future for large scale production, even if the primacy of one process or the other, in terms of cost and manufacturing effectiveness, has not been systematically demonstrated yet.

A. Single step deposition

Single step (SS) deposition of perovskite films represents a low cost and facile route towards high-performance PSCs. The perovskite absorber is deposited starting from a solution of both PbX_2 and CH_3NH_3X (X: I, Cl, Br) in a polar solvent, like DMF,[88] DMSO,[48,89] γ-butyrolactone (GBL),[90] or mixed solvents.[91] Spin coating is the most widely employed technique at lab scale, but others, suitable for large areas, such as blade[92,93] and slot die coating,[94] have also been demonstrated. An annealing process is then required to evaporate the solvent and crystallize the perovskite. It is typically carried out on a hot plate at 70-110 °C for several minutes up to few hours but can be dramatically reduced to few seconds or even to 1 ms by NIR[95] and photonic flash annealing,[96] respectively, delivering in both cases around 11% PCE in alumina-based cells with mixed halide perovskite.

The mixed halide $CH_3NH_3PbI_{3-x}Cl_x$ in a planar geometry has yielded 13.8% efficiency device[1] when spin-coated from a DMF solution, without any additives nor interface engineering and thermally annealed with spiro-OMeTAD as HTM. This was further enhanced to 15.9% in cells with an alumina scaffold[66] and to 19.3% by modification/doping of both ITO and compact TiO_2.[47]

Despite its simplicity, the key issue of SS deposition is the lack of control over the crystallization process, being affected by many factors, from the choice of solvents[90,91] and precursors to the surface properties of the substrate,[97,98] from the solvent evaporation during the deposition to the annealing conditions.[97,99] As a result, large morphological variations occur, leading to inhomogeneous, rough, and partially covered layers, which reduce light absorption and increase the carrier recombination rate, eventually causing a drop in both device efficiency and reproducibility.[100] Optimizing the perovskite film coverage and morphology in SS method is then crucial and many strategies have been reported so far, mainly to control the crystallization kinetics.

The use of additives to increase the solubility of the solid precursors in the solvent, such as hydriodic acid (HI), enables the formation of dense, pinhole-free perovskite films with high crystallinity, suppressing the formation of PbI_2 impurities, detected otherwise in films without HI, and thereby reducing the traps. By adding a small amount of HI (100 μl/ml) to the $MAPbI_3$ precursor solution in DMF, an efficiency as high as 18.1% in planar perovskite solar cells, based on PEDOT:PSS and PCBM, has been achieved.[101]

Other solution additives, such as morphology controllers (e.g., NH_4Cl,[102,103] 1,8-diiodooctane (DIO),[104,105] and N-cyclohexyl-2-pyrrolidone (CHP)[106]) benefit the crystallization of perovskite, slowing it down and leading to uniform coverage and crystallization of perovskite films.

Modified SS methods, based on solvent engineering, such as solvent dripping/drop-casting[48,107] and solvent-solvent extraction (or anti-solvent bath),[108,109] have been shown to lead to fast and controlled crystallization of extremely uniform and dense perovskite films. The solvent dripping method involves a different solvent from the one in the precursor solution, dripped on top of the wet film during the spin coating process to induce a fast crystallization of uniformly sized grains. Xiao *et al.*[107] reported dripping chlorobenzene onto a spinning $CH_3NH_3PbI_3$ film from a DMF solution giving rise to instantly flat, uniform layers, with large crystalline grains up to a micron in size yielding planar cells with PCE of over 13%. The second solvent rapidly reduces the solubility of $CH_3NH_3PbI_3$ in the mixed solvent and thereby promotes fast nucleation and growth of the crystals in the film, whose formation is complete within 1 min. Furthermore, only 10 min of annealing at 100 °C is needed to evaporate any residual solvent. For mesoporous cells, by Li-doping the TiO_2 and using mixed cations and halides in the precursor solution, PCE over 19% has been achieved.[110]

Similarly, by including in the precursor composition three different cations (Cs, MA, FA) and halides (Iodine, Bromine), a stabilized efficiency of 21.1% has been recently achieved via chlorobenzene dripping, followed by 1 h annealing at 100 °C, in cells with mesoporous TiO_2 and spiro-OMeTAD as HTM.[54] Zhu *et al.*[64] report a remarkable 18.8% efficiency for p-i-n planar cells, endowed with toluene-dripped MAPI films.

The solvent-solvent extraction[108] avoids the thermal annealing step of the standard SS route by immersing the perovskite film, immediately after the spin coating, in a bath of a low-boiling-point (anti) solvent, such as diethyl ether, at room temperature. The efficient extraction of the high-boiling-point solvent of the precursor solution, N-methyl-2-pyrrolidone (NMP), promotes rapid (within 2 min) crystallization of uniform, ultra-smooth, high quality perovskite films of controlled thicknesses. Zhou et al.[108] reported a PCE up to 15.2% for planar $CH_3NH_3PbI_3$ cells processed by this method, which is potentially suitable for roll-to-roll manufacturing, once the spin coating is replaced by other processes (spray, inkjet, and slot die).

The DSE[60] can also be regarded as SS deposition: the organic source (MAI) and the inorganic components ($PbCl_2$) are evaporated simultaneously from separate sources at 10^{-5} mbar followed by annealing. The resulting $CH_3NH_3PbI_{3-x}Cl_x$ films are extremely uniform and, incorporated in planar cells, show PCE of over 15%. Still the method is not easily scalable.

B. Double step deposition

The DS deposition of perovskite films in its first embodiment, introduced by Burschka[15] for mesoporous TiO_2 cells, with 15% efficiency, comprised the deposition of PbI_2 via spin coating followed by immersion into a solution of CH_3NH_3I and drying at 70 °C for 30 min. PbI_2 films converted instantaneously into $CH_3NH_3PbI_3$, enabling much better control over the film morphology and higher reproducibility than with standard SS deposition, as well as better pore filling and more conformal capping layer.[111] On the other hand, DS deposition presents some limitations such as additional process steps, even if already demonstrated on large area via scalable slot-die coating and roll-to-roll production,[112] and comparatively higher processing cost than for SS.

Further optimization has led to efficiencies exceeding 20%, by introducing onto the TiO_2 scaffold a mesoporous lead halide capping layer, which enables complete infiltration of the mixed cation solution resulting in rapid and full conversion to compact $FA_{1-x}MA_xPb(I_{1-x}Br_x)_3$ films.[113] Also for planar configuration, a nanostructured lead iodide layer facilitates the conversion to $CH_3NH_3PbI_3$, leading to smooth and PbI_2-free films with PCE of 16.21%. The immersion in MAI solution can be substituted by a VAVD in presence of solid MAI, demonstrated also for large areas,[114] or by MAI spin coating, followed by annealing in the presence of DMF vapour.[115]

A very interesting and effective DS approach is the intermolecular exchange process (IEP),[61] in which a mediator, i.e., DMSO, acts as both solvent and reactant for PbI_2, to prevent rapid and uncontrolled self-assembly crystallization between MAI or FAI and PbI_2. By spin coating a FAI solution on top of DMSO-intercalated-PbI_2 films, a direct molecular exchange of DMSO with FAI molecules occurs, producing large-grained $FAPbI_3$ films without residual PbI_2 and cells with efficiency greater than 20%.[61]

V. ISSUES IN PSCS—HYSTERESIS AND DEGRADATION OF PEROVSKITE SOLAR CELLS

Despite the remarkable achievements in PCE of PSCs, one of the crucial issues prior to its commercial deployment is the stability of the device that depends on several factors, both intrinsic, such as perovskite structural/chemical stability and extrinsic, i.e., moisture, oxygen, heat, light.[116,117] This limits their lifetime to few hundreds of hours only, as shown in Table III. To start with, the crystal structure of the perovskite should be intrinsically stable. $CH_3NH_3PbX_3$ materials are stable, both structurally and chemically, but still the hygroscopic nature of the organic cation causes moisture ingress and thus degradation. Mixing or substituting the MA cation with FA or Cs can improve the perovskite stability towards moisture and heat.[54,118] A recent in situ FTIR spectroscopy study reveals that the evaporation of MA during the film fabrication itself triggers the instability—hinting that the film fabrication is an important step for the stability of PSCs.[119]

Hysteresis, which is related to ionic motion in the perovskite and the nature of the contacts, can affect the photovoltaic characterization (i.e., variation in J-V curves for different scan rates) but it is unlikely detrimental in terms of device stability, even if it can worsen for devices stored/aged in air.[116] Oxidation and photo-oxidation have been observed for perovskite thin films but are less

TABLE III. Stability of representative perovskite solar cells under continuous light irradiation (RT = room temperature).

Cell structure	Encapsulation	Test duration	Temperature	Atmosphere	Humidity	Load	PCE degradation percentage	Reference
FTO/c-TiO$_2$/m-TiO$_2$/Cs$_x$M[a]/spiro-OMeTAD/Au	No	250 h	RT	N$_2$	...	Maximum power point	9% in the first few hours, then stable	[54]
FTO/c-TiO$_2$/Al$_2$O$_3$/CH$_3$NH$_3$PbI$_{3-X}$Cl$_X$/spiro-OMeTAD/Au	Epoxy resin + glass cover in glove box	1000 h	40 °C	Air	...	Open circuit	50% in the first 200 h, then stable	[67]
FTO/c-TiO$_2$/m-TiO$_2$/ZrO$_2$/(5-AVA)$_x$(MA)$_{1-x}$PbI$_3$/Carbon	No	1008 h	RT	Air	...	Open circuit	≈5%	[77]
FTO/c-TiO$_2$/FA$_{0.9}$Cs$_{0.1}$PbI$_3$/spiro-OMeTAD/Ag	UV curable sealant under N$_2$ atmosphere	220 h	<65 °C	Air	<50%	Open circuit	30%	[118]
FTO/oxo-G$_1$[b]/CH$_3$NH$_3$PbI$_3$/PCBM/ZnO/Al	No	1000 h (0.5 sun)	RT	Air	30%-50%	Open circuit	40%	[120]
FTO/C$_{60}$/CH$_3$NH$_3$PbI$_3$/spiro-OMeTAD/Au	Hot melt polymer foil in a N$_2$ filled glove box	500 h	60 °C	Air	...	Maximum power point	10%	[122]
FTO/c-TiO$_2$/ Al$_2$O$_3$/CH$_3$NH$_3$PbI$_3$/spiro-OMeTAD/Al$_2$O$_3$/Au	Yes	576 h	RT	Air	50%	Open circuit	10%	[126]
FTO/c-TiO$_2$/m-TiO$_2$/ZrO$_2$/(5-AVA)$_x$(MA)$_{1-x}$PbI$_3$/Carbon	Thin glass sheet, Surlyn spacer and epoxy resin	7 days – outdoor (Saudi Arabia)	35-42 °C	Air	...	...	Stable	[132]

[a]Cs$_x$M = Cs$_x$(MA$_{0.17}$FA$_{0.83}$)$_{(100-x)}$Pb(I$_{0.83}$Br$_{0.17}$)$_3$ with x = 5.
[b]oxo-G$_1$ = oxo-functionalized graphene.

severe in complete devices, depending on the hydrophobicity of the top layer[120,121] and can be avoided by proper encapsulation under inert conditions, which enables cells to be stable for up to 1000 h.[67,73,122]

Perovskite rapid degradation to water and even air moisture represents a huge concern. The degradation mechanism is a partially reversible hydration process, which leads to irreversible PbI_2 formation after prolonged exposure to moisture.[123] It can be dramatically accelerated by heat and electric field, and also in presence of photodose,[124,125] which confirms the need for effective encapsulation and/or moisture resistant layers, such as buffer layers between perovskite and HTM,[126,127] moisture-blocking HTMs,[128] and hydrophobic carbon electrodes.[77] In terms of photo-stability, UV light seems to represent a threat for TiO_2-based devices, through the surface adsorbed oxygen, which is desorbed under UV illumination, leaving behind trap sites acting as recombination centers.[67] Also, the perovskite layer is found to be reactive to anatase TiO_2 nanoparticle scaffold or a flat counterpart that leads to ion migration across the interface[129,130] whereas no degradation is observed for TiO_2 nanorods based devices[130] that offer crystalline morphology and a thermodynamically stable rutile phase.[114,131]

On the other hand, TiO_2-based devices show very rapid degradation in ambient conditions, induced by (white LED) light and oxygen,[133] in particular by photogenerated superoxides causing deprotonation of the methylammonium cation.[134] The three-layered monolithic structure that does include a TiO_2 film represents an exception. Different reports demonstrate remarkable long-term stability for this architecture under different conditions, from simulated AM 1.5 sunlight[77] to real outdoor conditions.[132] The thick carbon layer, a good oxygen absorber, likely provides an additional supply of oxygen, it acts as a barrier and hosts a sort of "sacrificial" perovskite, infiltrated throughout its thickness.[116] Finally, planar heterojunction cells have been reported to be promising for long-term operation.[101,122]

As long as the materials are chosen carefully and the devices are properly encapsulated, the intrinsic and extrinsic factors of degradation could be overtaken. Additional efforts are needed to optimize active materials, identify effective encapsulation strategies (that can be borrowed from OPV or OLED technology), and define standard protocols for testing long-term stability so that results from a wide research community can be compared.

A. Hysteresis in perovskite solar cells

The *J–V* curves of PSCs typically show a dependency on the measurement conditions such as scan direction, rate and range, and voltage pre-treatment.[23,135] This often leads to difficulty in reporting true performance of the device as the PCE is overestimated when scanning from forward-to-reverse voltage sweep direction. The origin of this anomalous hysteresis is still under debate, the plausible cause being the ferroelectric properties of halide perovskites, their ionic-electronic transport, slow ion migration, dynamic trapping and de-trapping of photogenerated charges and also due the charge accumulation at TiO_2-perovskite interface.[135–141] We refer to a comprehensive review for further details on the origin of *J–V* hysteresis and its elimination.[142] We also note its strong dependency on the ESC/HSC, device architecture, processing conditions of perovskite, and so forth. For example, replacement of TiO_2 with PCBM or C_{60} as an ESC reduced hysteresis significantly.[143,144] The fact that most high efficiency PSCs (both the planar and mesoporous) do not show any hysteresis points to the urgent need for optimizing the device architectures and interfacial layers and also the processing conditions, which would lead to efficient and stable PSCs.

VI. OUTLOOK

Solution processable perovskite solar cells of efficiency >20% provide much hope for a clean energy for planet Earth; however, few unsolved issues prevent them from practically deployed—most important of which is its challenging operational stability. To develop a stable device, one would understand the origin of this instability, which in turn requires a clear understanding on the mechanism of photovoltaic action in this device. A wide variety of available device architecture

of perovskite solar cells could puzzle about the role of interfacial energetics towards origin of PV parameters. For example, an understanding of literature shows that the open circuit voltage although is determined by the splitting of quasi-Fermi levels of perovskite, the extent of splitting is largely influenced by the interfacing selective contact. Furthermore, significant efforts have been undertaken to discover and eliminate hysteresis in the current–voltage characteristics of the cell while measuring the photovoltaic parameters in the forward and the reverse bias conditions. Consequently, another "school of thought" that *eliminating hysteresis would lead to stable device* has also been followed currently. Besides operational stability, perovskite solar cells have environmental and economic drawbacks: crystal chemistry of hybrid perovskites requires toxic and less abundant materials (such as lead) for them to be photoactive. Could photoactive perovskites be synthesized from less toxic and highly abundant materials? Also, the hybrid perovskites crystallized on insulating scaffolds also show high photoconversion efficiency in devices, giving further opportunity to optimize ideal crystals suitable choice of materials and synthesis methods. Thus, more in-depth analysis will be necessary in future to see the full potential of perovskite solar cells and may also give us the possibility to design new materials with similar extraordinary properties.

ACKNOWLEDGMENTS

[1] NERL, Best research cell efficiencies, 2016.

[2] H. S. Kim, C. R. Lee, J. H. Im, K. B. Lee, T. Moehl, A. Marchioro, S. J. Moon, R. Humphry-Baker, J. H. Yum, J. E. Moser, M. Grätzel, and N. G. Park, Sci Rep. **2**, 591 (2012).

[3] M. A. Green, A. Ho-Baillie, and H. J. Snaith, Nat. Photonics **8**(7), 506–514 (2014).

[4] H. Snaith and L. Schmidt-Mende, APL Mater. **2**, 081201 (2014).

[5] P. Gao, M. Grätzel, and M. K. Nazeeruddin, Energy Environ. Sci. **7**(8), 2448–2463 (2014).

[6] P. P. Boix, S. Agarwala, T. M. Koh, N. Mathews, and S. G. Mhaisalkar, J. Phys. Chem. Lett. **6**(5), 898–907 (2015).

[7] H. S. Jung and N. G. Park, Small **11**(1), 10–25 (2015).

[8] C. C. Stoumpos, C. D. Malliakas, and M. G. Kanatzidis, Inorg. Chem. **52**, 9019–9038 (2013).

[9] Y. Yamada, T. Nakamura, M. Endo, A. Wakamiya, and Y. Kanemitsu, Appl. Phys. Express **7**(3), 032302 (2014).

[10] J. M. Ball, S. D. Stranks, M. T. Hörantner, S. Hüttner, W. Zhang, E. J. W. Crossland, I. Ramirez, M. Riede, M. B. Johnston, R. H. Friend, and H. J. Snaith, Energy Environ. Sci. **8**(2), 602–609 (2015).

[11] J. M. Ball, M. M. Lee, A. Hey, and H. J. Snaith, Energy Environ. Sci. **6**(6), 1739–1743 (2013).

[12] B. Conings, L. Baeten, T. Jacobs, R. Dera, J. D'Haen, J. Manca, and H.-G. Boyen, APL Mater. **2**, 081505 (2014).

[13] G. Xing, N. Mathews, S. S. Lim, N. Yantara, X. Liu, D. Sabba, M. Grätzel, S. Mhaisalkar, and T. C. Sum, Nat. Mater. **13**, 476–480 (2014).

[14] F. Di Giacomo, A. Fakharuddin, R. Jose, and T. M. Brown, "Progress, challenges and perspectives in flexible perovskite solar cells," Energy Environ. Sci. (to be published).

[15] J. Burschka, N. Pellet, S. J. Moon, R. Humphry-Baker, P. Gao, M. K. Nazeeruddin, and M. Grätzel, Nature **499**(7458), 316–319 (2013).

[16] T. Zhang, M. Yang, Y. Zhao, and K. Zhu, Nano Lett. **15**(6), 3959–3963 (2015).

[17] M. Saba, M. Cadelano, D. Marongiu, F. Chen, V. Sarritzu, N. Sestu, C. Figus, M. Aresti, R. Piras, A. Geddo Lehmann, C. Cannas, A. Musinu, F. Quochi, A. Mura, and G. Bongiovanni, Nat. Commun. **5**, 5049 (2014).

[18] G. Xing, N. Mathews, S. Sun, S. S. Lim, Y. M. Lam, M. Graïzel, S. Mhaisalkar, and T. C. Sum, Science **342**(6156), 344–347 (2013).

[19] S. Brittman, G. W. P. Adhyaksa, and E. C. Garnett, MRS Commun. **5**(1), 7–26 (2015).

[20] L. Serrano-Lujan, N. Espinosa, T. T. Larsen-Olsen, J. Abad, A. Urbina, and F. C. Krebs, Adv. Energy Mater. **5**(20), 1501119 (2015).

[21] R. S. Sanchez, V. Gonzalez-Pedro, J. W. Lee, N. G. Park, Y. S. Kang, I. Mora-Sero, and J. Bisquert, J. Phys. Chem. Lett. **5**(13), 2357–2363 (2014).

[22] Y. Shao, Z. Xiao, C. Bi, Y. Yuan, and J. Huang, Nat. Commun. **5**, 5784 (2014).

[23] H. J. Snaith, A. Abate, J. M. Ball, G. E. Eperon, T. Leijtens, N. K. Noel, S. D. Stranks, J. T. W. Wang, K. Wojciechowski, and W. Zhang, J. Phys. Chem. Lett. **5**(9), 1511–1515 (2014).

[24] F. Brivio, A. B. Walker, and A. Walsh, APL Mater. **1**(4), 042111 (2013).

[25] B. Saparov and D. B. Mitzi, Chem. Rev. **116**(7), 4558–4596 (2016).

[26] A. Glazer, Acta Crystallogr., Sect. B **28**(11), 3384–3392 (1972).

[27] R. M. Hazen, Sci. Am. **258**, 74 (1988).

[28] A. Amat, E. Mosconi, E. Ronca, C. Quarti, P. Umari, M. K. Nazeeruddin, M. Grätzel, and F. De Angelis, Nano Lett. **14**(6), 3608–3616 (2014).

29 C. C. Stoumpos and M. G. Kanatzidis, Acc. Chem. Res. **48**, 2791–2802 (2015).
30 J. M. Frost, K. T. Butler, and A. Walsh, APL Mater. **2**, 081506 (2014).
31 J. C. Johnson, Z. Li, P. F. Ndione, and K. Zhu, J. Mater. Chem. C **4**(22), 4847–4852 (2016).
32 B. S. Kalanoor, L. Gouda, R. Gottesman, S. Tirosh, E. Haltzi, A. Zaban, and Y. R. Tischler, ACS Photonics **3**(3), 361–370 (2016).
33 R. Zhang, J. Fan, X. Zhang, H. Yu, H. Zhang, Y. Mai, T. Xu, J. Wang, and H. J. Snaith, ACS Photonics **3**(3), 371–377 (2016).
34 M. Hirasawa, T. Ishihara, T. Goto, K. Uchida, and N. Miura, Physica B **201**, 427–430 (1994).
35 K. Tanaka, T. Takahashi, T. Ban, T. Kondo, K. Uchida, and N. Miura, Solid State Commun. **127**(9-10), 619–623 (2003).
36 Q. Lin, A. Armin, R. C. R. Nagiri, P. L. Burn, and P. Meredith, Nat. Photonics **9**(2), 106–112 (2015).
37 E. J. Juarez-Perez, R. S. Sanchez, L. Badia, G. Garcia-Belmonte, Y. Soo Kang, I. Mora-Sero, and J. Bisquert, J. Phys. Chem. Lett. **5**, 2390–2394 (2014).
38 K. Liang, D. B. Mitzi, and M. T. Prikas, Chem. Mater. **10**(1), 403–411 (1998).
39 J. H. Im, J. Chung, S. J. Kim, and N. G. Park, Nanoscale Res. Lett. **7**, 1–14 (2012).
40 T. Baikie, Y. Fang, J. M. Kadro, M. Schreyer, F. Wei, S. G. Mhaisalkar, M. Graetzel, and T. J. White, J. Mater. Chem. A **1**(18), 5628–5641 (2013).
41 A. M. A. Leguy, J. M. Frost, A. P. McMahon, V. G. Sakai, W. Kochelmann, C. Law, X. Li, F. Foglia, A. Walsh, B. C. O'Regan, J. Nelson, J. T. Cabral, and P. R. F. Barnes, Nat. Commun. **6**, 7124 (2015).
42 J. Even, L. Pedesseau, and C. Katan, J. Phys. Chem. C **118**(22), 11566–11572 (2014).
43 S. Zhao, C. Lan, J. Ma, S. S. Pandey, S. Hayase, and T. Ma, Solid State Commun. **213-214**, 19–23 (2015).
44 X. Zhu, H. Su, R. A. Marcus, and M. E. Michel-Beyerle, J. Phys. Chem. Lett. **5**(17), 3061–3065 (2014).
45 A. Buin, R. Comin, J. Xu, A. H. Ip, and E. H. Sargent, Chem. Mater. **27**(12), 4405–4412 (2015).
46 M. Saliba, S. Orlandi, T. Matsui, S. Aghazada, M. Cavazzini, J.-P. Correa-Baena, P. Gao, R. Scopelliti, E. Mosconi, K.-H. Dahmen, F. De Angelis, A. Abate, A. Hagfeldt, G. Pozzi, M. Graetzel, and M. K. Nazeeruddin, Nat. Energy **1**, 15017 (2016).
47 H. Zhou, Q. Chen, G. Li, S. Luo, T. B. Song, H. S. Duan, Z. Hong, J. You, Y. Liu, and Y. Yang, Science **345**(6196), 542–546 (2014).
48 N. J. Jeon, J. H. Noh, Y. C. Kim, W. S. Yang, S. Ryu, and S. I. Seok, Nat. Mater. **13**(9), 897–903 (2014).
49 E. Edri, S. Kirmayer, M. Kulbak, G. Hodes, and D. Cahen, J. Phys. Chem. Lett. **5**(3), 429–433 (2014).
50 C. G. Wu, C. H. Chiang, and S. H. Chang, Nanoscale **8**(7), 4077–4085 (2016).
51 S. S. Mali, C. S. Shim, and C. K. Hong, NPG Asia Mater. **7**, e208 (2015).
52 G. E. Eperon, G. M. Paterno, R. J. Sutton, A. Zampetti, A. A. Haghighirad, F. Cacialli, and H. J. Snaith, J. Mater. Chem. A **3**(39), 19688–19695 (2015).
53 D. Bi, W. Tress, M. I. Dar, P. Gao, J. Luo, C. Renevier, K. Schenk, A. Abate, F. Giordano, J.-P. Correa Baena, J.-D. Decoppet, S. M. Zakeeruddin, M. K. Nazeeruddin, M. Grätzel, and A. Hagfeldt, Sci. Adv. **2**(1), e1501170 (2016).
54 M. Saliba, T. Matsui, J.-Y. Seo, K. Domanski, J.-P. Correa-Baena, M. K. Nazeeruddin, S. M. Zakeeruddin, W. Tress, A. Abate, A. Hagfeldt, and M. Gratzel, Energ. Environ. Sci. **9**, 1989–1997 (2016).
55 N. K. Noel, S. D. Stranks, A. Abate, C. Wehrenfennig, S. Guarnera, A.-A. Haghighirad, A. Sadhanala, G. E. Eperon, S. K. Pathak, M. B. Johnston, A. Petrozza, L. M. Herz, and H. J. Snaith, Energy Environ. Sci. **7**(9), 3061–3068 (2014).
56 D. Li, H. Wu, H.-C. Cheng, G. Wang, Y. Huang, and X. Duan, ACS Nano **10**, 6933 (2016).
57 C. Eames, J. M. Frost, P. R. F. Barnes, B. C. O'Regan, A. Walsh, and M. S. Islam, Nat. Commun. **6**, 7497 (2015).
58 A. Kojima, K. Teshima, Y. Shirai, and T. Miyasaka, J. Am. Chem. Soc. **131**(17), 6050–6051 (2009).
59 J. H. Im, C. R. Lee, J. W. Lee, S. W. Park, and N. G. Park, Nanoscale **3**(10), 4088–4093 (2011).
60 M. Liu, M. B. Johnston, and H. J. Snaith, Nature **501**, 395–398 (2013).
61 W. S. Yang, J. H. Noh, N. J. Jeon, Y. C. Kim, S. Ryu, J. Seo, and S. I. Seok, Science **348**(6240), 1234–1237 (2015).
62 N. Ahn, D. Y. Son, I. H. Jang, S. M. Kang, M. Choi, and N. G. Park, J. Am. Chem. Soc. **137**(27), 8696–8699 (2015).
63 M. Park, J.-Y. Kim, H. J. Son, C.-H. Lee, S. S. Jang, and M. J. Ko, Nano Energy **26**, 208–215 (2016).
64 Z. G. Zhu, Y. Bai, X. Liu, C.-C. Chueh, S. Yang, and A. K. Y. Jen, Adv. Mater. **28**, 6478–6484 (2016).
65 C. Bi, Q. Wang, Y. Shao, Y. Yuan, Z. Xiao, and J. Huang, Nat. Commun. **6**, 7747 (2015).
66 K. Wojciechowski, M. Saliba, T. Leijtens, A. Abate, and H. J. Snaith, Energy Environ. Sci. **7**(3), 1142–1147 (2014).
67 T. Leijtens, G. E. Eperon, S. Pathak, A. Abate, M. M. Lee, and H. J. Snaith, Nat. Commun. **4**, 2885 (2013).
68 J. P. Correa Baena, L. Steier, W. Tress, M. Saliba, S. Neutzner, T. Matsui, F. Giordano, T. J. Jacobsson, A. R. Srimath Kandada, S. M. Zakeeruddin, A. Petrozza, A. Abate, M. K. Nazeeruddin, M. Gratzel, and A. Hagfeldt, Energy Environ. Sci. **8**(10), 2928–2934 (2015).
69 Q. Hu, J. Wu, C. Jiang, T. Liu, X. Que, R. Zhu, and Q. Gong, ACS Nano **8**(10), 10161–10167 (2014).
70 H. Wei, J. Xiao, Y. Yang, S. Lv, J. Shi, X. Xu, J. Dong, Y. Luo, D. Li, and Q. Meng, Carbon **93**, 861–868 (2015).
71 Z. Wei, H. Chen, K. Yan, X. Zheng, and S. Yang, J. Mater. Chem. A **3**(48), 24226–24231 (2015).
72 V. Gonzalez-Pedro, E. J. Juarez-Perez, W.-S. Arsyad, E. M. Barea, F. Fabregat-Santiago, I. Mora-Sero, and J. Bisquert, Nano Lett. **14**, 888–893 (2014).
73 M. M. Lee, J. Teuscher, T. Miyasaka, T. N. Murakami, and H. J. Snaith, Science **338**(6107), 643–647 (2012).
74 S. D. Stranks, G. E. Eperon, G. Grancini, C. Menelaou, M. J. P. Alcocer, T. Leijtens, L. M. Herz, A. Petrozza, and H. J. Snaith, Science **342**(6156), 341–344 (2013).
75 D. Liu, J. Yang, and T. L. Kelly, J. Am. Chem. Soc. **136**(49), 17116–17122 (2014).
76 B. E. Cohen, S. Gamliel, and L. Etgar, APL Mater. **2**(8), 081502 (2014).
77 A. Mei, X. Li, L. Liu, Z. Ku, T. Liu, Y. Rong, M. Xu, M. Hu, J. Chen, Y. Yang, M. Gratzel, and H. Han, Science **345**, 295–298 (2014).
78 Y. Li, S. Ye, W. Sun, W. Yan, Y. Li, Z. Bian, Z. Liu, S. Wang, and C. Huang, J. Mater. Chem. A **3**(36), 18389–18394 (2015).
79 J. You, L. Meng, T. B. Song, T. F. Guo, W. H. Chang, Z. Hong, H. Chen, H. Zhou, Q. Chen, Y. Liu, N. De Marco, and Y. Yang, Nat. Nanotechnol. **11**(1), 75–81 (2016).

[80] Q. Wali, A. Fakharuddin, I. Ahmed, M. H. Ab Rahim, J. Ismail, and R. Jose, J. Mater. Chem. A **2**(41), 17427–17434 (2014).

[81] Q. Wali, A. Fakharuddin, and R. Jose, J. Power Sources **293**, 1039–1052 (2015).

[82] Q. Wali, A. Fakharuddin, A. Yasin, M. H. Ab Rahim, J. Ismail, and R. Jose, J. Alloys Compd. **646**, 32–39 (2015).

[83] J. H. Heo, D. H. Song, and S. H. Im, Adv. Mater. **26**(48), 8179–8183 (2014).

[84] S. Ryu, J. H. Noh, N. J. Jeon, Y. Chan Kim, W. S. Yang, J. Seo, and S. I. Seok, Energy Environ. Sci. **7**(8), 2614–2618 (2014).

[85] W. H. Nguyen, C. D. Bailie, E. L. Unger, and M. D. McGehee, J. Am. Chem. Soc. **136**(31), 10996–11001 (2014).

[86] E. Edri, S. Kirmayer, D. Cahen, and G. Hodes, J. Phys. Chem. Lett. **4**(6), 897–902 (2013).

[87] M. Kröger, S. Hamwi, J. Meyer, T. Riedl, W. Kowalsky, and A. Kahn, Org. Electron. **10**(5), 932–938 (2009).

[88] D. Shen, X. Yu, X. Cai, M. Peng, Y. Ma, X. Su, L. Xiao, and D. Zou, J. Mater. Chem. A **2**(48), 20454–20461 (2014).

[89] B. Conings, L. Baeten, C. De Dobbelaere, J. D'Haen, J. Manca, and H. G. Boyen, Adv. Mater. **26**(13), 2041–2046 (2014).

[90] J. Y. Jeng, Y. F. Chiang, M. H. Lee, S. R. Peng, T. F. Guo, P. Chen, and T. C. Wen, Adv. Mater. **25**(27), 3727–3732 (2013).

[91] H. B. Kim, H. Choi, J. Jeong, S. Kim, B. Walker, S. Song, and J. Y. Kim, Nanoscale **6**(12), 6679–6683 (2014).

[92] S. Razza, F. Di Giacomo, F. Matteocci, L. Cinà, A. L. Palma, S. Casaluci, P. Cameron, A. D'Epifanio, S. Licoccia, A. Reale, T. M. Brown, and A. Di Carlo, J. Power Sources **277**, 286 (2014).

[93] Z. Yang, C.-C. Chueh, F. Zuo, J. H. Kim, P.-W. Liang, and A. K. Y. Jen, Adv. Energy Mater. **5**(13), 1500328 (2015).

[94] T. M. Schmidt, T. T. Larsen-Olsen, J. E. Carlé, D. Angmo, and F. C. Krebs, Adv. Energy Mater. **5**(15), 1500569 (2015).

[95] J. Troughton, C. Charbonneau, M. J. Carnie, M. L. Davies, D. A. Worsley, and T. M. Watson, J. Mater. Chem. A **3**(17), 9123–9127 (2015).

[96] J. Troughton, M. J. Carnie, M. L. Davies, C. Charbonneau, E. H. Jewell, D. A. Worsley, and T. M. Watson, J. Mater. Chem. A **4**(9), 3471–3476 (2016).

[97] G. E. Eperon, V. M. Burlakov, P. Docampo, A. Goriely, and H. J. Snaith, Adv. Func. Mater. **24**(1), 151–157 (2014).

[98] S. Colella, E. Mosconi, P. Fedeli, A. Listorti, F. Gazza, F. Orlandi, P. Ferro, T. Besagni, A. Rizzo, G. Calestani, G. Gigli, F. De Angelis, and R. Mosca, Chem. Mater. **25**(22), 4613–4618 (2013).

[99] F. Wang, D. Meng, X. Li, Z. Zhu, Z. Fu, and Y. Lu, Appl. Surf. Sci. **357**, 391–396 (2015).

[100] J. H. Im, H. S. Kim, and N. G. Park, APL Mater. **2**(8), 081510 (2014).

[101] J. H. Heo, H. J. Han, D. Kim, T. K. Ahn, and S. H. Im, Energy Environ. Sci. **8**(5), 1602–1608 (2015).

[102] Y. Chen, Y. Zhao, and Z. Liang, Chem. Mater. **27**(5), 1448–1451 (2015).

[103] C. Zuo and L. Ding, Nanoscale **6**(17), 9935–9938 (2014).

[104] P. W. Liang, C. Y. Liao, C. C. Chueh, F. Zuo, S. T. Williams, X. K. Xin, J. Lin, and A. K. Y. Jen, Adv. Mater. **26**(22), 3748–3754 (2014).

[105] C. C. Chueh, C. Y. Liao, F. Zuo, S. T. Williams, P. W. Liang, and A. K. Y. Jen, J. Mater. Chem. A **3**(17), 9058–9062 (2015).

[106] Y. J. Jeon, S. Lee, R. Kang, J. E. Kim, J. S. Yeo, S. H. Lee, S. S. Kim, J. M. Yun, and D. Y. Kim, Sci. Rep. **4**, 6953 (2014).

[107] M. Xiao, F. Huang, W. Huang, Y. Dkhissi, Y. Zhu, J. Etheridge, A. Gray-Weale, U. Bach, Y. B. Cheng, and L. Spiccia, Angew. Chem., Int. Ed. **53**(37), 9898–9903 (2014).

[108] Y. Zhou, M. Yang, W. Wu, A. L. Vasiliev, K. Zhu, and N. P. Padture, J. Mater. Chem. A **3**(15), 8178–8184 (2015).

[109] Y. Zhou, M. Yang, O. S. Game, W. Wu, J. Kwun, M. A. Strauss, Y. Yan, J. Huang, K. Zhu, and N. P. Padture, ACS Appl. Mater. Interfaces **8**(3), 2232–2237 (2016).

[110] F. Giordano, A. Abate, J. P. Correa Baena, M. Saliba, T. Matsui, S. H. Im, S. M. Zakeeruddin, M. K. Nazeeruddin, A. Hagfeldt, and M. Graetzel, Nat. Commun. **7**, 10379 (2016).

[111] N. Yantara, D. Sabba, F. Yanan, J. M. Kadro, T. Moehl, P. P. Boix, S. Mhaisalkar, M. Grätzel, and C. Grätzel, Chem. Commun. **51**(22), 4603–4606 (2015).

[112] K. Hwang, Y. S. Jung, Y. J. Heo, F. H. Scholes, S. E. Watkins, J. Subbiah, D. J. Jones, D. Y. Kim, and D. Vak, Adv. Mater. **27**(7), 1241–1247 (2015).

[113] C. Yi, X. Li, J. Luo, S. M. Zakeeruddin, and M. Grätzel, Adv. Mater. **28**(15), 2964–2970 (2016).

[114] A. Fakharuddin, A. L. Palma, F. D. Giacomo, S. Casaluci, F. Matteocci, Q. Wali, M. Rauf, A. D. Carlo, T. M. Brown, and R. Jose, Nanotechnology **26**(49), 494002 (2015).

[115] Z. Xiao, Q. Dong, C. Bi, Y. Shao, Y. Yuan, and J. Huang, Adv. Mater. **26**, 6503 (2014).

[116] T. Leijtens, G. E. Eperon, N. K. Noel, S. N. Habisreutinger, A. Petrozza, and H. J. Snaith, Adv. Energy Mater. **5**(20), 1500963 (2015).

[117] T. A. Berhe, W. N. Su, C. H. Chen, C. J. Pan, J. H. Cheng, H. M. Chen, M. C. Tsai, L. Y. Chen, A. A. Dubale, and B. J. Hwang, Energy Environ. Sci. **9**(2), 323–356 (2016).

[118] J.-W. Lee, D.-H. Kim, H.-S. Kim, S.-W. Seo, S. M. Cho, and N.-G. Park, Adv. Energy Mater. **5**(20), 1501310 (2015).

[119] C. Manspeaker, P. Scruggs, J. Preiss, D. A. Lyashenko, and A. A. Zakhidov, J. Phys. Chem. C **120**(12), 6377–6382 (2016).

[120] H. Chen, Y. Hou, C. E. Halbig, S. Chen, H. Zhang, N. Li, F. Guo, X. Tang, N. Gasparini, I. Levchuk, S. Kahmann, C. O. Ramirez Quiroz, A. Osvet, S. Eigler, and C. J. Brabec, J. Mater. Chem. A **4**, 11604 (2016).

[121] L. Zheng, Y. H. Chung, Y. Ma, L. Zhang, L. Xiao, Z. Chen, S. Wang, B. Qu, and Q. Gong, Chem. Commun. **50**(76), 11196–11199 (2014).

[122] K. Wojciechowski, T. Leijtens, S. Spirova, C. Schlueter, M. Hoerantner, J. T.-W. Wang, C.-Z. Li, A. K.-Y. Jen, T.-L. Lee, and H. J. Snaith, J. Phys. Chem. Lett. **6**, 2399–2405 (2015).

[123] A. Leguy, Y. Hu, M. Campoy-Quiles, M. I. Alonso, O. J. Weber, P. Azarhoosh, M. van Schilfgaarde, M. T. Weller, T. Bein, J. Nelson, P. Docampo, and P. R. F. Barnes, Chem. Mater. **27**(9), 3397–3407 (2015).

[124] F. Matsumoto, S. M. Vorpahl, J. Q. Banks, E. Sengupta, and D. S. Ginger, J. Phys. Chem. C **119**(36), 20810–20816 (2015).

[125] N. A. Manshor, Q. Wali, K. K. Wong, S. K. Muzakir, A. Fakharuddin, L. Schmidt-Mende, and R. Jose, Phys. Chem. Chem. Phys. **18**, 21629 (2016).

[126] S. Guarnera, A. Abate, W. Zhang, J. M. Foster, G. Richardson, A. Petrozza, and H. J. Snaith, J. Phys. Chem. Lett. **6**(3), 432–437 (2015).

[127] X. Dong, X. Fang, M. Lv, B. Lin, S. Zhang, J. Ding, and N. Yuan, J. Mater. Chem. A **3**(10), 5360–5367 (2015).

[128] S. N. Habisreutinger, T. Leijtens, G. E. Eperon, S. D. Stranks, R. J. Nicholas, and H. J. Snaith, Nano Lett. **14**(10), 5561–5568 (2014).

[129] A. Fakharuddin, F. Di Giacomo, I. Ahmed, Q. Wali, T. M. Brown, and R. Jose, J. Power Sources **283**, 61–67 (2015).

[130] A. Fakharuddin, F. Di Giacomo, A. L. Palma, F. Matteocci, I. Ahmed, S. Razza, A. D'Epifanio, S. Licoccia, J. Ismail, A. Di Carlo, T. M. Brown, and R. Jose, ACS Nano **9**(8), 8420–8429 (2015).

[131] I. Ahmed, A. Fakharuddin, Q. Wali, A. R. B. Zainun, J. Ismail, and R. Jose, Nanotechnology **26**(10), 105401 (2015).

[132] X. Li, M. Tschumi, H. Han, S. S. Babkair, R. A. Alzubaydi, A. A. Ansari, S. S. Habib, M. K. Nazeeruddin, S. M. Zakeeruddin, and M. Grätzel, Energy Technol. **3**, 551–555 (2015).

[133] D. Bryant, N. Aristidou, S. Pont, I. Sanchez-Molina, T. Chotchunangatchaval, S. Wheeler, J. R. Durrant, and S. A. Haque, Energy Environ. Sci. **9**(5), 1655–1660 (2016).

[134] N. Aristidou, I. Sanchez-Molina, T. Chotchuangchutchaval, M. Brown, L. Martinez, T. Rath, and S. A. Haque, Angew. Chem., Int. Ed. **54**, 8208–8212 (2015).

[135] E. L. Unger, E. T. Hoke, C. D. Bailie, W. H. Nguyen, A. R. Bowring, T. Heumüller, M. G. Christoforod, and M. D. McGehee, Energy Environ. Sci. **7**, 3690–3698 (2014).

[136] J. Wei, Y. Zhao, H. Li, G. Li, J. Pan, D. Xu, Q. Zhao, and D. Yu, J. Phys. Chem. Lett. **5**, 3937–3945 (2014).

[137] H.-W. Chen, N. Sakai, M. Ikegami, and T. Miyasaka, J. Phys. Chem. Lett. **6**, 164–169 (2015).

[138] A. Dualeh, T. Moehl, N. Tétreault, J. Teuscher, P. Gao, M. K. Nazeeruddin, and M. Grätzel, ACS Nano **8**, 362–373 (2014).

[139] Y. Yang, J. Xiao, H. Wei, L. Zhu, D. Li, Y. Luo, H. Wu, and Q. Meng, RSC Adv. **4**(95), 52825–52830 (2014).

[140] O. Almora, I. Zarazua, E. Mas-Marza, I. Mora-Sero, J. Bisquert, and G. Garcia-Belmonte, J. Phys. Chem. Lett. **6**, 1645–1652 (2015).

[141] B. Chen, M. Yang, X. Zheng, C. Wu, W. Li, Y. Yan, J. Bisquert, G. Garcia-Belmonte, K. Zhu, and S. Priya, J. Phys. Chem. Lett. **6**, 4693–4700 (2015).

[142] B. Chen, M. Yang, S. Priya, and K. Zhu, J. Phys. Chem. Lett. **7**(5), 905–917 (2016).

[143] K. Wojciechowski, S. D. Stranks, A. Abate, G. Sadoughi, A. Sadhanala, N. Kopidakis, G. Rumbles, C.-Z. Li, R. H. Friend, A. K.-Y. Jen, and H. J. Snaith, ACS Nano **8**, 12701–12709 (2014).

[144] J. W. Seo, S. Park, Y. C. Kim, N. J. Jeon, J. H. Noh, S. C. Yoon, and S. I. Seok, Energy Environ. Sci. **7**, 2642–2646 (2014).

[145] M. Grätzel, Nat. Mater. **13**, 838–842 (2014).